Int J Fract (2006) 141:447–457
DOI 10.1007/s10704-006-9006-9

ORIGINAL PAPER

# Compression-induced axial crack propagation in DCDC polymer samples: experiments and modeling

**Thomas A. Plaisted · Alireza V. Amirkhizi · Sia Nemat-Nasser**

Received: 21 February 2006 / Accepted: 10 July 2006 / Published online: 25 October 2006


**Abstract** The fracture strength of PMMA is studied using columns with rectangular cross-section that contain a central hole and are subjected to axial compression. Samples with geometries such that the width is 2, 3, 4, and 5 times the diameter of the hole are investigated. Cracks are initiated by introducing sharp notches in the axial direction at the crowns of the hole in each sample. The sample is then subjected to axial compression such that the axial cracks grow in a stable manner until a critical compression is attained, after which the cracks extend rapidly in the sample but do not reach its ends. To predict the experimental results, we have first sought to use several published models, but discovered that none would produce results in accord with our data, as they seem not to address the essential features of our beam-column experiments. We have then developed a simple model that consists of a suitably modified version of an elasticity solution based on a short-crack in an infinite plate, combined with a beam-column solution for a long-crack. This model yields results in good accord with our data and also gives reasonable values for the fracture toughness of the material. A comparative discussion of several published models is presented at the end of the paper, pointing out that linear elasticity is not an appropriate tool for solving the present beam-column problem.

**Keywords** DCDC · Polymer fracture · Crack growth

T.A. Plaisted · A.V. Amirkhizi · S. Nemat-Nasser (✉)
Center of Excellence for Advanced Materials,
Department of Mechanical and Aerospace
Engineering, University of California,
San Diego, CA,USA
e-mail: sia@ucsd.edu

## 1 Introduction

The *double cleavage drilled compression* sample (DCDC) refers to a column of a rectangular cross-section with a circular hole drilled through its center that is subjected to axial compression. This technique provides many advantages in studying the fracture toughness of brittle materials. Janssen (1974) originally introduced the specimen for measuring the fracture toughness of glass. Under a uniform axial compression, a tensile stress is produced at the crowns of the hole, as indicated in Fig. 1. Once the tensile stress reaches the fracture strength of the material, a stable mode I crack is generated at each crown, propagating along the mid-plane of the sample as the axial compression is increased. When the crack reaches a critical length, it may jump and extend the entire length of the sample with a minute increase in the axial compression, being arrested close to the ends of the column due to the geometric constraint imposed by the frictional forces acting over the ends of the sample in contact with the loading platens. By careful

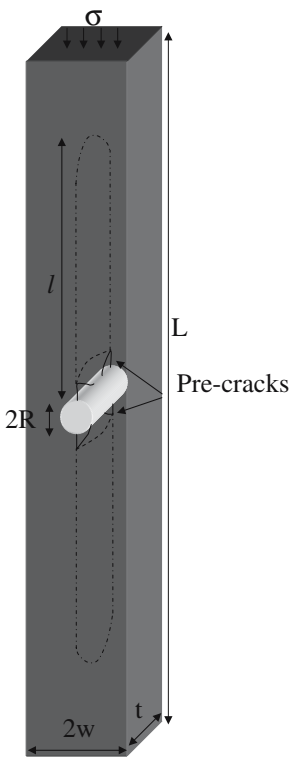


**Fig. 1** DCDC specimen with central hole. Solid lines emanating from the crowns of the hole indicate the shape and location of the initial pre-cracks. Upon loading, pre-cracks connect and propagate (dotted lines) towards the direction of applied compression

displacement-controlled loading, the crack growth can be controlled to a certain extent.

We have identified this specimen geometry to be ideal for studying the healing of polymers (Chen et al. 2002, 2003), since the fractured interface may be closely repositioned to its original location for the healing process, after which it is re-fractured in order to measure the fracture toughness of the healed crack. As a starting point, we have performed a series of quantitative tests on PMMA samples, and have sought to model the tests using expressions reported in the literature, e.g., by Sammis and Ashby (1986), Warren (1987), Michalske et al. (1993), He et al. (1995), and Jenne et al. (2003). The results of these published models did not correspond well to our experimental data, whereas a simple model that combines a suitably modified version of two estimates, one based on a short-crack and the other on a long-crack approximation, correlates well with all our experimental results and yields a reasonable range of values for the fracture toughness. These results are reported in the present paper. In seeking to use the published models, we have realized that the two-dimensional linear elasticity solutions, used to obtain results in several of the above mentioned models, do not actually apply to the present problem, since compression-induced axial crack growth in DCDC samples is strongly affected by the cross-sectional rotation and the resulting lateral deflection of the column. These kinematical quantities are ignored as second-order terms in linear elasticity, rendering linear elasticity an inappropriate tool for modeling the compression-induced axial fracturing in beam-column samples. This and related issues are examined at the end of the paper. While Sammis and Ashby (1986) do seek to include the beam-column effects, their result does not apply to large crack lengths relative to the hole radius; see the Discussion section for further detail.

In Sect. 2, the experimental procedures and sample dimensions are presented. The experimental results are given in Sect. 3. In Sect. 4, we have detailed our modeling procedure for both the short- and long-crack solutions, and the results are compared with those of our experiments. A comparative discussion is then presented in Sect. 5, and the resulting conclusions are outlined in Sect. 6. The results of the healing polymer will be reported elsewhere.

## 2 Experimental procedure

The DCDC specimen in this study were machined from Chemcast Acrylic poly(methylmethacrylate) plates. Sample geometries with half-width to hole radius ($w/R$) ratios of 2, 3, 4, and 5 were investigated. The dimensions, as labeled in Fig. 1, were as follows: hole radius, $R$, ranged from 1.6 mm to 2.6 mm, sample half-width, $w$, from 4 mm to 8 mm, thickness, $t$, 11 mm, and length, $L$, 50 and 100 mm. The specific dimensions for each specimen are listed in Table 1. The upper and lower surfaces of each specimen in contact with the loading platens were polished flat and parallel to within 0.013 mm. The sample dimensions were originally selected due to the availability of numerical

**Table 1** Specimen dimensions

| Dimensions (mm) | | | | | | Dimensions (mm) | | | | | |
|---|---|---|---|---|---|---|---|---|---|---|---|
| Specimen | $L$ | $2w$ | $t$ | $R$ | $w/R$ | Specimen | $L$ | $2w$ | $t$ | $R$ | $w/R$ |
| 1 | 100 | 8 | 11 | 2 | 2 | 15 | 100 | 16 | 11 | 2.6 | 3 |
| 2 | 100 | 8 | 11 | 2 | 2 | 16 | 100 | 16 | 11 | 2.6 | 3 |
| 3 | 100 | 8 | 11 | 2 | 2 | 17 | 100 | 16 | 11 | 2 | 4 |
| 4 | 100 | 8 | 11 | 2 | 2 | 18 | 100 | 16 | 11 | 2 | 4 |
| 5 | 50 | 8 | 11 | 2 | 2 | 19 | 100 | 16 | 11 | 2 | 4 |
| 6 | 50 | 8 | 11 | 2 | 2 | 20 | 50 | 16 | 11 | 2 | 4 |
| 7 | 50 | 8 | 11 | 2 | 2 | 21 | 50 | 16 | 11 | 2 | 4 |
| 8 | 100 | 12 | 11 | 2 | 3 | 22 | 50 | 16 | 11 | 2 | 4 |
| 9 | 100 | 12 | 11 | 2 | 3 | 23 | 50 | 16 | 11 | 2 | 4 |
| 10 | 100 | 12 | 11 | 2 | 3 | 24 | 50 | 16 | 11 | 2 | 4 |
| 11 | 50 | 12 | 11 | 2 | 3 | 25 | 50 | 16 | 11 | 1.6 | 5 |
| 12 | 50 | 12 | 11 | 2 | 3 | 26 | 50 | 16 | 11 | 1.6 | 5 |
| 13 | 50 | 12 | 11 | 2 | 3 | 27 | 50 | 16 | 11 | 1.6 | 5 |
| 14 | 50 | 12 | 11 | 2 | 3 | 28 | 50 | 16 | 11 | 1.6 | 5 |

relations previously derived by He et al. (1995) for samples with similar dimensional ratios, using numerical simulations and linear elasticity. However, since the results of this model, as well as other published models that we examined, did not correlate with our experimental data, samples with other dimensions were produced and tested in order to identify potential sources of the discrepancy.

Previous work in this area indicated difficulty in growing stable cracks in PMMA using the DCDC sample geometry (Idonije et al. 1993; Jenne et al. 2003). In other materials, such a glass, it is often reported that the crack initiates at the crowns of the hole without the presence of a starter notch (Janssen 1974; Michalske and Fuller 1985; Crichton et al. 1999), while in polymers such as PMMA, a starter notch is necessary to initiate cracking at the crowns. Various schemes were undertaken in an effort to initiate a stable crack. Samples were notched along the entire length of the upper and lower crowns of the hole with a 0.2 mm diamond wire saw. Likewise samples were scored along the entire length of the upper and lower crowns with a razor blade. A combination of these two methods was also attempted, where the crowns were notched through the sample thickness with the wire saw and subsequently scored with a razor blade. In each case a crack propagated from the upper and lower crowns, though the crack growth was highly unstable and resulted in the crack extending rapidly to the far extremes of the sample length, similar to previous experiments by Idonije et al. (1993).

A successful method was developed, however, by wedging a razor blade into the material to create an actual crack, rather than a scratch or notch, at the crowns of the hole. A curved blade was fixed in an end-mill and positioned above the sample such that it extended beyond the diameter of the hole by 0.25 mm. The blade was pressed into the hole to a depth of about 1 mm at the upper and lower crown of the hole for both the front and back surfaces of the specimen. This method was successful in wedging open and propagating a crack, though this could only be achieved close to the surface of the specimen; see Fig. 1. Hence the pre-crack was not continuous through the thickness of the sample. However, during each test, as load was gradually applied to the specimen, the crack would first grow through the thickness of the sample until it formed a continuous crack front through the thickness of the specimen. It would then grow towards the direction of the applied compression in a stable manner. This would happen at both pre-notched crowns of the hole.

Samples were loaded quasi-statically in an Instron Model 1332 universal testing machine in displacement control with an 88 kN load cell. An external camera (Nikon D100) was focused at 4× magnification on the specimen. Each sample was compressed at a rate of 1.3 $\mu$m/s. The test was paused every 25 $\mu$m in displacement, for a duration of about 10 s, so that the peak load over that period could be recorded along with a picture. The extended pause was implemented to ensure the

crack propagation had equilibrated prior to each photo. The crack length in each photo was later measured graphically by pixel counting software and correlated to the applied load.

## 3 Experimental results

The typical compression test proceeded in the following way: after an initial buildup of strain within the specimen, the pre-crack would grow through the thickness to form a uniform crack front; the crack front would then grow in linear relation with the applied load and in a stable manner such that multiple data points could be obtained. This relation would taper off at some plateau stress whereby the crack would grow rapidly with little additional applied stress. In the stable region, there was little crack-opening displacement across the width of the sample. Upon reaching the plateau stress, the sample would bend outward due to the presence of a non-uniform stress distribution over the narrowest cross-section of the beam, resulting in a diamond shaped opening. The picture sequence in Fig. 2 illustrates the propagation in a typical sample.

The crack front was observed to grow in a characteristic parabola shape similar to that observed in other DCDC experiments, indicative of the transition from plane strain at the center to plane stress at the faces (Janssen 1974). The crack length, $l$, was measured from the top of the hole to the maximum extent of the crack in the direction of the applied compression, which was conveniently facilitated by the transparent nature of PMMA. The initial pre-cracks at the crowns of the hole were less than 1 mm in length. Crack length measurements were recorded only when the two starter cracks on the front and back faces had joined up and the parabolic crack front was observed. This shape was evident by the time the crack had reached a length of about 2 mm. The crack length, $l$, was recorded as the average of the top and bottom crack lengths for each photo, typically within a few percent of each other over the course of the experiment.

Crack propagation was more controllable and the results more repeatable for specimens with larger $w/R$ ratio. For samples with $w/R$ of 2, the crack would grow to a length of about 2 mm and then rapidly extend to the full length of the sample. Samples with a $w/R$ of 3, 4 and 5 exhibited stable crack growth over a greater range. Beyond a critical load, however, the crack would also grow rapidly. Samples with $w/R$ of 5 demonstrated the most stable and repeatable crack growth. The results for all tests are shown in Figs. 3 and 4, in terms of applied stress versus normalized crack length.

For $w/R$ ratios 2, 3 and 4, two different sample lengths (50 mm and 100 mm) were investigated.

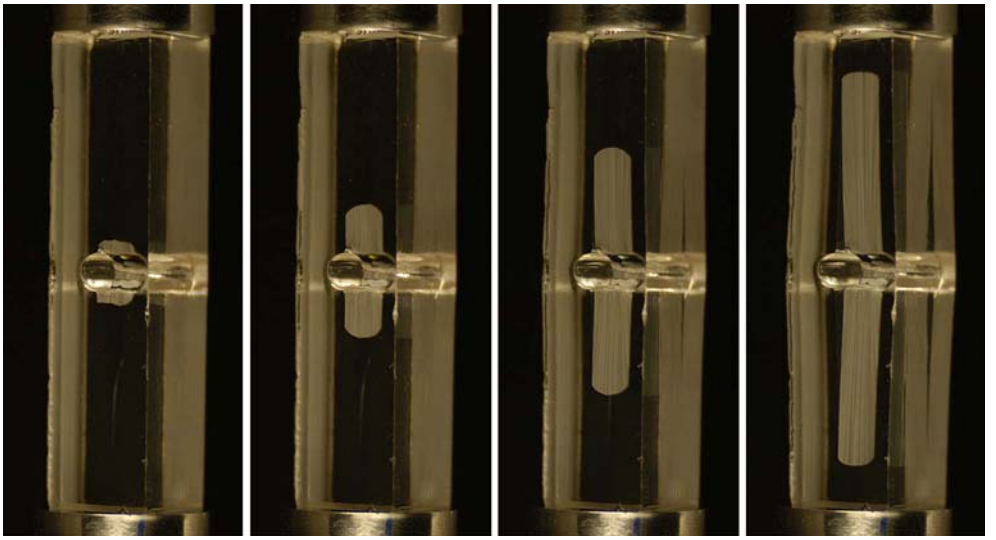

**Fig. 2** Picture sequence, from left to right, of advancing crack. The third picture from the left shows the sample loaded well into the plateau regime. Sample is viewed from same perspective as shown in Fig. 1

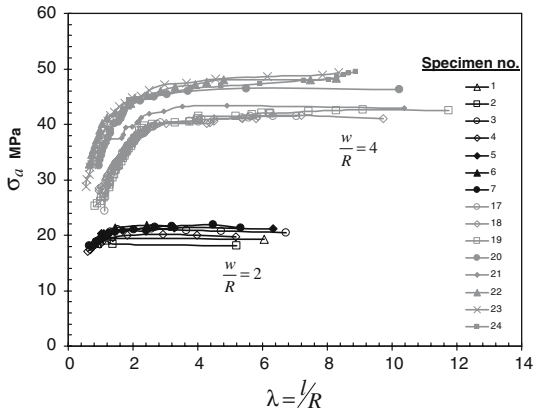


**Fig. 3** Experimental data for specimens with $w/R$ ratios 2 and 4

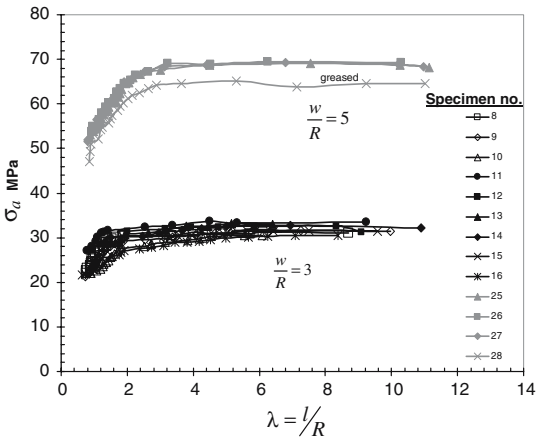


**Fig. 4** Experimental data for specimens with $w/R$ ratios 3 and 5

Long samples with a $w/R$ ratio of 5 could not be tested due to buckling induced by the increased stress required to drive the crack in this geometry. Sample length had an effect on the results, where the longer samples required less stress to reach the plateau region. This effect is most evident in the results for samples with $w/R$ of 4, where the plateau region of longer samples 17, 18 and 19 was less than the shorter specimen 20–24. This is attributed to friction at the sample ends in contact with the loading platens that acts to confine the sample laterally and oppose the crack opening tensile force. In the longer samples this confining force is located further from the crack front and thus has less effect compared to the shorter samples. To verify this, we performed a single test (specimen 28) where the platen surfaces were coated with a thin layer of lubricating grease to reduce the friction. As expected, the sample reached the plateau region at a lower applied stress compared to the results from otherwise identical specimens 25, 26 and 27. The effect of relative sample width and hole diameter was shown to have no significant effect. The sample width and hole diameter were increased proportionately in samples 15 and 16 compared to samples 8, 9, and 10, such that a $w/R$ ratio of 3 was maintained in all specimen. The results for these tests fell within the experimental fluctuation for this $w/R$ ratio such that no difference was observed.

## 4 Modeling

In this section we develop a simple yet accurate analytical model for describing the propagation of a crack in a polymer DCDC specimen under uniaxial compression. The calculations are straightforward and do not require the finite-element simulations that have recently been used by Jenne et al. (2003). The model reproduces the experimental results more accurately than any of the other published models that we have sought to use, (e.g., Sammis 1986; He et al. 1995; Jenne et al. 2003). Some possible causes of this are examined at the end of the paper.

To simplify the modeling, we consider two extreme cases: a short-crack regime and a long-crack regime. In the DCDC test, the normal stress required to extend the crack increases with the crack length in the short-crack regime, whereas a load plateau exists in the long-crack regime with little additional stress being required to substantially increase the crack length. The onset of this plateau designates the boundary between the "short" and "long" crack regimes. There is of course a small transition regime that we do not address in our modeling.

To model the short-crack, first consider the Green's function for a slit crack in an infinite plate subjected to two pairs of concentrated forces, as shown in Fig. 5. The resulting stress intensity factor is (Erdogan 1962),

$$K = \frac{P}{\sqrt{\pi a}}\left(\sqrt{\frac{a+x}{a-x}} + \sqrt{\frac{a-x}{a+x}}\right). \quad (1)$$

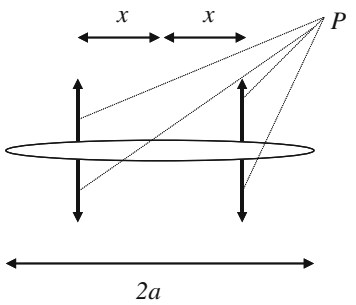


**Fig. 5** Representation of a slit crack with symmetric concentrated loads

Then note that, in the absence of cracks, a hole in an infinite plate subjected to axial compression induces the following tensile stresses over the interval $R < |x| < R\sqrt{3}$ on the plane $y = 0$:

$$\sigma_{yy}(x) = \sigma_{\mathrm{a}} \left( -\frac{1}{2(x/R)^2} + \frac{3}{2(x/R)^4} \right). \tag{2}$$

Here $\sigma_{\mathrm{a}}$ denotes the applied axial stress. In what follows, we identify $\sigma_{\mathrm{a}}$ with the applied axial load when the crack length is $l$, and, for this reason, henceforth we denote $\sigma_{\mathrm{a}}$ by $\sigma_0(l)$. The stress intensity factor at the tip of a slit crack of length $2(l + R)$ in an infinite plate, subjected to internal opening stresses $\sigma_{yy}(x)$ over the interval $R < |x| < R\sqrt{3}$, is

$$\begin{aligned} K &= \int_R^{R\sqrt{3}} \frac{\sigma_{yy}(x)}{\sqrt{\pi(l+R)}} \left( \sqrt{\frac{l+R+x}{l+R-x}} + \sqrt{\frac{l+R-x}{l+R+x}} \right) \mathrm{d}x \\ &= \frac{\sigma_0(l)\sqrt{R}}{\sqrt{\pi(1+\lambda)}} \int_1^{\sqrt{3}} \left( -\frac{1}{2\xi^2} + \frac{3}{2\xi^4} \right) \\ &\quad \times \left( \sqrt{\frac{1+\lambda+\xi}{1+\lambda-\xi}} + \sqrt{\frac{1+\lambda-\xi}{1+\lambda+\xi}} \right) \mathrm{d}\xi. \end{aligned} \tag{3}$$

Here $\lambda = l/R$. The integral can be evaluated numerically. Note that for $l > R\sqrt{3}$, $\sigma_{yy}(x)$ is compressive, and hence does not affect the stress intensity factor. A good approximation is achieved by replacing the stress distribution with an equivalent concentrated force, $P$, acting at a distance $x$,

$$P = Rd\sigma_{\mathrm{a}}(l), \quad x = eR. \tag{4,5}$$

The magnitude, $P$, and the point of the application, $x$, of this force are estimated by integrating the stress distribution in (2). This gives,

$$d = \frac{\sqrt{3}}{9} \sim 0.19254, \quad e = \frac{3\sqrt{3}}{4}(2 - \ln 3) \sim 1.1709. \tag{6, 7}$$

The stress intensity factor due to this concentrated force is a very good approximation of Eq. 3. It yields,

$$K = \frac{d\sigma_0(l)\sqrt{R}}{\sqrt{\pi(1+\lambda)}} \left( \sqrt{\frac{1+\lambda+e}{1+\lambda-e}} + \sqrt{\frac{1+\lambda-e}{1+\lambda+e}} \right). \tag{8}$$

Comparison between this and the more complicated form (3) shows little deviation. The non-dimensional version of this equation is,

$$\frac{\sigma_0(l)\sqrt{w}}{K_{\mathrm{c}}} = \frac{\sqrt{w/R}\sqrt{\pi(1+\lambda)}}{d\left( \sqrt{\frac{1+\lambda+e}{1+\lambda-e}} + \sqrt{\frac{1+\lambda-e}{1+\lambda+e}} \right)}. \tag{9}$$

We now seek to modify and apply this equation to the actual problem shown in Fig. 6, where relatively short cracks extend from the crowns of a circular hole in a beam of finite width, $2w$, under axial compression. To account for the effect of the finite width, we now view the parameter $d$ as a scaling factor and allow it to be a function of $w/R$. When the ratio $w/R$ becomes very large, the value of $d(w/R)$ is expected to approach that of Eq. 6, calculated based on the Green's function of an unbounded medium. As $w/R$ decreases, we expect $d(w/R)$ to increase since the presence of the hole in a finite-width sample promotes crack growth under axial compression. Equivalently, the

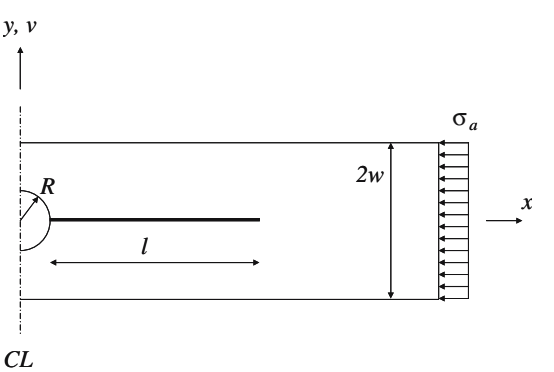


**Fig. 6** Schematics and dimensions of the DCDC model

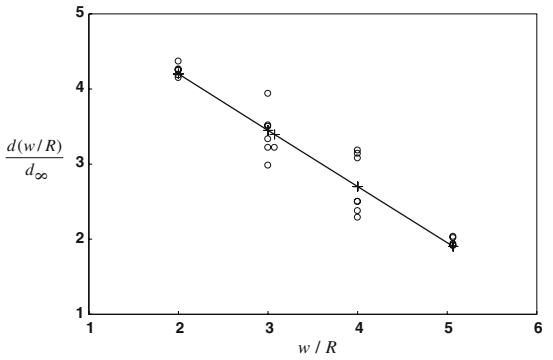


**Fig. 7** Normalized values of $d(w/R)$ with respect to the theoretical prediction in an infinite plate

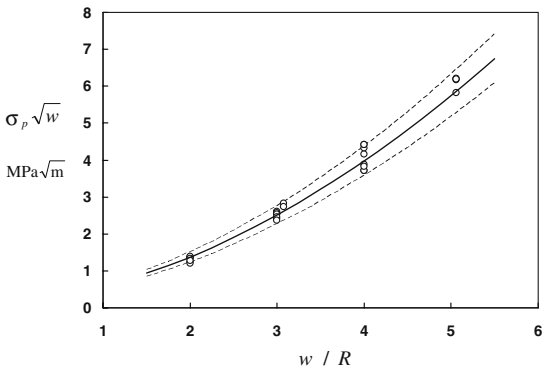


**Fig. 8** Plateau stress vs. $w/R$ ratio. The circles are the experimentally measured values. The solid curve represents the model result for a critical stress intensity factor of $K_{\text{IC}} = 0.71\,\text{MPa}\sqrt{m}$, while the dashed curves are for a 10% variation, i.e., $K_{\text{IC}} = 0.64,\ 0.78\,\text{MPa}\sqrt{m}$

stress intensity factor at the crack tip will tend to be larger. For an average critical stress intensity factor of $K_{\text{IC}} = 0.71\,\text{MPa}\sqrt{m}$, calculated from the long-crack model (discussed below), the normalized values of $d(w/R)$ with respect to the theoretical value of Eq. 6 for an infinite plate shown in Fig. 7 reproduce the experimental results with small error, up to the point where the axial stress approaches the limiting value of the long-crack model. As expected, $d(w/R)$ is a monotonically decreasing function of $w/R$, approaching unity in the limit of very large $w/R$. Since we are concerned with relatively small values of $w/R$ associated with our beam-column samples, we may use a linear fit within the considered range, arriving at,

$$\frac{d(w/R)}{d_\infty} = 5.7 - 0.75\frac{w}{R}. \tag{10}$$

Note that this fit is only useful for the range of geometries studied here.

When the crack is suitably long, we use an Euler–Bernoulli beam model with appropriate boundary conditions applied to one quarter of the sample. The deflection of the beam is defined by the following boundary-value problem:

$$\frac{\mathrm{d}^2}{\mathrm{d}x^2}\left(EI\frac{\mathrm{d}^2 v}{\mathrm{d}x^2}\right) = 0, \quad v(x = l + R) = 0,$$

$$\frac{\mathrm{d}v}{\mathrm{d}x}(x = l + R) = 0, \tag{11-13}$$

$$\frac{\mathrm{d}v}{\mathrm{d}x}(x = 0) = 0, \quad EI\frac{\mathrm{d}^2 v}{\mathrm{d}x^2}(x = 0) = M_0. \tag{14, 15}$$

Here $v(x)$ is the deflection of the beam at point $x$, measured normal to the axis of the beam; $E$ is the Young's modulus of the sample; $I$ is the area moment of inertia of the cross-section; and $M_0$ is the moment induced at the end of the beam due to the non-uniform axial stress distribution at $x = 0$, over the section $R < y < w$. Since the beam is long relative to the hole radius, we take $I$ to be constant throughout the entire length of the beam, ignoring the reduced cross-section at the hole, i.e., we set $I = bw^3/12$, where $b$ is the sample thickness. The resulting bending moment in the beam is,

$$M(x; l) = EI\frac{\mathrm{d}^2 v}{\mathrm{d}x^2}(x) = M_0\left(1 - 2\frac{x}{l + R}\right), \tag{16}$$

and the bending energy, the resulting energy release rate (per unit area), and the stress intensity factor respectively become,

$$E(l) = \int_0^{l+R} \frac{\left[M(x; l)\right]^2}{2EIb}\,\mathrm{d}x, \quad G(l) = 2\frac{\partial E}{\partial l},$$

$$K = \sqrt{EG} = \frac{2M_0}{bw^{3/2}}. \tag{17–19}$$

The factor 2 appears in Eq. 18 since we have considered one quarter of the sample when there are actually two beams contributing to the energy release rate at the crack tip.

Note that, in this regime, $M_0$ does not change as the crack grows. As the beam deforms under the axial compression, the bending moment at the end of the beam does not change with the increasing deflection. When the crack length is large compared to the hole radius and the width of the sample,

$l/R \gg 1$ and $l/w \gg 1$, the stress field at the crack tip does not change with crack growth. Since $M_0$ depends on the ratio $w/R$, to apply the results to samples with various $w/R$, we now express this bending moment in terms of a non-dimensional function, $g(w/R)$, as follows:

$$M_0(R, w) = \sigma_p b w R g(w/R). \tag{20}$$

Here $\sigma_p$ is the axial stress applied to the sample in the plateau regime. The plateau stress and the critical stress intensity factor are related by

$$\frac{\sigma_p \sqrt{w}}{K_c} = \frac{w/R}{2g(w/R)}. \tag{21}$$

To calculate the function $g$, we assume that the axial stress on the plane $x = 0$ consists of two parts, as follows:

$$\sigma_{xx}(y) = -\sigma_p \left[ \left( 1 + \frac{1}{2(y/R)^2} + \frac{3}{2(y/R)^4} \right) + \frac{(\alpha w - \beta R) + (\beta - \alpha) y}{w - R} \right]. \tag{22}$$

The first part corresponds to the terms inside the parentheses within the brackets on the right-hand side. It represents the compressive stresses transmitted on the plane $x = 0$ near a hole in an infinite plate. The second part is the last term within the brackets, and corresponds to a superposed linear stress distribution. We determine the parameters $\alpha$ and $\beta$ such that the resultant moment due to this term, taken about the neutral axis $y = w/2$, is zero. This condition together with the requirement of axial equilibrium, yields the following expressions for these parameters:

$$\alpha = \frac{(R/w)^2 (1 + (R/w)^2)(4(R/w) - 1)}{(1 - R/w)^2}, \tag{23}$$

$$\beta = \frac{(R/w)^2 (1 + (R/w)^2)(2(R/w) + 1)}{(1 - R/w)^2}. \tag{24}$$

Calculating the bending moment about the neutral axis, $y = w/2$, we obtain the function $g(w/R)$,

$$g(w/R) = \frac{3 + 2\ln(w/R)}{4(w/R)} - \frac{1}{4(w/R)^3}. \tag{25}$$

Equations 21 and 25 now give the final model estimate of the normalized axial stress corresponding to the plateau stress for samples of various geometries. Using the experimental results when the crack is suitably long, we have obtained an *average* value for the critical stress intensity factor for this material, i.e., $K_{IC} = 0.71\,\text{MPa}\sqrt{m}$. The value of the critical stress intensity factor obtained in this manner for all our tests lies within 10% of this value and well within the range of critical stress intensity factors given in the literature for PMMA (Marshall and Williams 1973). In Fig. 8 we have plotted the product of the plateau stress and $w^{1/2}$ versus the $w/R$ ratio, for $K_{IC} = 0.71,\ \ 0.64,\ \ 0.78\,\text{MPa}\sqrt{m}$, i.e., the average (solid curve) and the average plus and minus 10% (dashed curves). The model estimates closely follow the experimental results for all test geometries. Figures 9 and 10 compare the short- and long-crack model results with the experimental data.

## 5 Discussion

Here we compare our experimental and analytical results with other published work. We focus on Michalske et al. (1993) and He et al. (1995), but the following comments apply also to all the models based on linear elasticity and linear finite-element solutions. In the present case, linear elasticity predicts a monotonically decreasing stress intensity factor at the tip of the crack as the crack length $l$ increases, thus requiring a monotonically increasing axial compression to drive the crack in a material

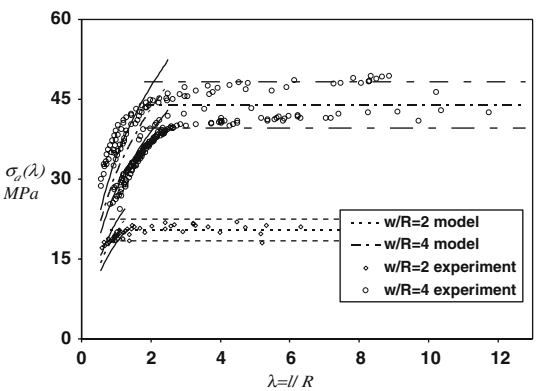


**Fig. 9** Axial load versus normalized crack length for $w/R = 2$ and 4: The solid and dashed curves represent the model results for the indicated values of $w/R$, using the critical stress intensity factors $K_{IC} = 0.71\,\text{MPa}\sqrt{m}$ and $K_{IC} = 0.64,\ \ 0.78\,\text{MPa}\sqrt{m}$. The initial curved segment is the short-crack solution and the flat line is the asymptotic long-crack solution

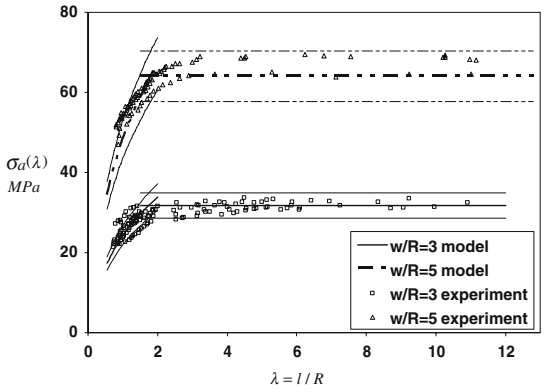


**Fig. 10** Axial load versus normalized crack length for $w/R = 3$ and 5: The solid and dashed curves represent the model results for the indicated values of $w/R$, using the critical stress intensity factors $K_{\rm IC} = 0.71\,{\rm MPa}\sqrt{m}$ and $K_{\rm IC} = 0.64,\quad 0.78\,{\rm MPa}\sqrt{m}$. The initial curved segment is the short-crack solution and the flat line is the asymptotic long-crack solution

with a constant critical value of the stress intensity factor. Using linearly elastic finite-element numerical simulations, He et al. (1995) for example find a linear relation between the (normalized) required axial stress and the (normalized) crack length. An examination of Fig. 6 in their paper shows a stress distribution around the hole that produces a (normalized) bending moment, taken about the neutral axis of the beam, which decreases by a factor of 8 when the crack length changes from $a/R = 2$ to $a/R = 14$; we have used a similar finite-element calculation to confirm this trend.

However, in a beam with a central hole under axial compression, the lateral deflection at the hole produces an effective bending moment that cannot be captured by the infinitesimal deformation assumed in linear elasticity since the deflection is a second-order quantity. For very stiff materials, this lateral deflection is very small, as may have been the case in the works of Michalske et al. (1993) and Turner et al. (1995), yet should have become evident had the crack been further extended in a sufficiently long sample. Michalske et al. (1993) tested fused silica ($E = 94\,{\rm GPa}$, $K_{\rm IC} = 0.74\,{\rm MPa}\sqrt{m}$) in ultra high vacuum and incrementally extended the crack by superimposing short duration stress pulses on a constant axial stress of sufficiently small value that would not extend the crack in the absence of the impulse. Turner et al. (1995) examined interface crack growth in a glass-epoxy-glass specimen ($\Gamma_{\rm ic}$ =24 J/m$^2$, $K_{\rm IC} = 1.29\,{\rm MPa}\sqrt{m}$), using soda-lime glass ($E = 69\,{\rm GPa}$). They also examined interface crack growth in a sapphire–gold–sapphire specimen ($\Gamma_{\rm ic}$ =10 J/m$^2$, $K_{\rm IC} = 1.97\,{\rm MPa}\sqrt{m}$), and a sapphire–platinum–sapphire specimen ($\Gamma_{\rm ic}$=30–52 J/m$^2$, $K_{\rm IC} = 3.42 - 4.5\,{\rm MPa}\sqrt{m}$), with sapphire having a Young's modulus of $E = 390\,{\rm GPa}$. Like our experiments, the load was monotonically increased after an initial pre-crack had been established. The materials tested in these experiments were comparatively stiff with low interface fracture toughness, which masked the second-order effects evident in our experiments.

In our beam-column analysis, we have assumed, for a sufficiently long crack, that the presence of the hole creates a bending moment on the cross-section at $x = 0$ (i.e., at the hole) that is not affected by the crack length. With this assumption, we have shown that the beam-column model, based on a strength-of-material approach, does indeed produce results that are in accord with the experimental data, using a constant value for the critical stress intensity factor that is within the expected range, hence suggesting that this simple model includes the essential physical features necessary to capture the essence of the experiments. Alternatively, one may consider a beam-column boundary-value problem and obtain a more accurate expression for the bending moment, as follows:

$$M(x) = M_0(\cos qx - \frac{\sin ql}{1 - \cos ql}\sin qx), \tag{26}$$

where $q^2 = P/EI$. This gives a stress intensity factor of

$$K = \frac{2\sqrt{3}M_0}{bw^{3/2}}\sqrt{1 - \frac{\sin ql(ql - \sin ql)}{(1 - \cos ql)^2}}, \tag{27}$$

which, similar to the previous results, is a very slowly varying function of $l$ for $ql < 1/3$. In fact, for $ql = 1/3$ (less than the largest value of the corresponding quantity in our experiments), Eq. 27 is to within 1% of (19). Furthermore, $K(l)$ in Eq. 27 is a very slowly increasing function of the crack length, which demonstrates the stability of the crack growth, as has been observed in our experiments; this may be partially evident in Figs. 3 and 4 that show, for most experiments, very slightly increasing fracture stress with increasing crack

length, in the plateau regime; this may be more evident for data in Fig. 9 corresponding to $w/R = 4$. The moment distribution and related deformation also show that the deflection around the hole is a local phenomenon and does not change when the crack length is increased, suggesting that the constant moment assumption is validated. An extended analysis by Jenne et al. (2003) uses a similar approach, based on the work by Sammis and Ashby (1986). Sammis and Ashby use a strength-of-material approach to study the effect on a plate's compressive uniaxial stress–strain relation, due to axial cracks that emanate from the crowns of circular holes that are periodically distributed in an infinite linearly elastic plate. Their calculations, however, are flawed by the incorrect estimate of an integral, for which they assume that the crack length is infinitesimally small relative to the radius of the hole and then apply the results to cases where the crack length exceeds 10 times the hole radius. Remarkably, this error leads to results that nicely correlate with the experimental observations on rock failure, but unfortunately does not follow from the correct solution of their model. This has been pointed out by Isida and Nemat-Nasser (1987) who provide the correct elasticity solution which shows that the common length of the axial cracks in such situations (infinite linearly elastic plate with periodic hole–crack distribution) has only a second-order effect on the axial stress–strain relation and hence it can have no relation to the experimental results on rock failure in compression.

## 6 Conclusions

Fracture studies of brittle polymer PMMA have been conducted using DCDC specimens. Pre-cracking and loading procedures were developed to propagate a stable crack from the upper and lower crowns of a central hole in a beam of rectangular cross-section subjected to axial compression. Stable crack growth was achieved until a plateau stress was reached, at which stage the resulting bending moment caused the crack to grow rapidly. We have sought to model the test results using expressions reported in the literature, but discovered that none of the published models that we considered produced results in accord with our experimental data. Thus, we developed a simple model that combines a suitably modified version of two estimates, one based on a short-crack and the other on a long-crack approximation. This model produces results in good accord with all our experimental results and also yields a reasonable value for the fracture toughness of the material. We have examined with care some of the published models and have discovered that those which are based on finite-element linear elasticity solutions are inappropriate tools for solving the present problem, since linear elasticity cannot capture the second-order effect due to the rotation of the cross-section of the beam, which is crucial to the correct estimate of a beam-column response.

## References

Chen X, Dam MA, Ono K, Mal A, Hongbin S, Nutt SR, Sheran K, Wudl F (2002) A thermally re-mendable cross-linked polymeric material. Science 295(5560):1698–1702

Chen X, Wudl F, Mal A, Hongbin S, Nutt SR (2003) New thermally remendable highly cross-linked polymeric materials. Macromolecules 36:1802–1807

Crichton SN, Tomozawa M, Hayden JS, Suratwala TI, Campbell JH (1999) Subcritical crack growth in a phosphate laser glass. J Am Ceramic Soc 82(11): 3097–3104

Erdogan F (1962) On the stress distribution in plates with collinear cuts under arbitrary loads. Proceedings of the Fourth U.S. National Congress of Applied Mechanics

He MY, Turner MR, Evans AG (1995) Analysis of the double cleavage drilled compression specimen for interface fracture energy measurements over a range of mode mixities. Acta Metallurgica Materialia 43(9):3453–3458

Idonije K, Motuku M, Shehata I, Aglan H (1993) Evaluation of the stress intensity factor of brittle polymers based on the crack arrest concept. J Reinforced Plastics Composites 12(7):778–786

Isida M, Nemat-Nasser S (1987) On mechanics of crack growth and its effects on the overall response of brittle porous solids. Acta Metallurgica 35(12):2887–2898

Janssen C (1974) Specimen for fracture mechanics studies on glass. 10th International Congress on Glass, Kyoto, Japan, Ceramic Society of Japan

Jenne TA, Keat WD, Larson MC (2003) Limits of crack growth stability in the double cleavage drilled compression specimen. Eng Fracture Mech 70(13): 1697–1719

Marshall GP, Williams JG (1973) The correlation of fracture data for pmma. J Mater Sci 8(1):138–140

Michalske TA, Fuller ER Jr (1985) Closure and repropagation of healed cracks in silicate glass. J Am Ceramic Soc 68(11):586–590

Michalske TA, Smith WL, Chen EP (1993) Stress intensity calibration for the double cleavage drilled compression specimen. Eng Fracture Mech 45(5): 637–642

Sammis CG, Ashby MF (1986) The failure of brittle porous solids under compressive stress states. Acta Metallurgica 34(3):511–526

Turner MR, Dalgleish BJ, He MY, Evans AG (1995) A fracture resistance measurement method for bimaterial interfaces having large debond energy. Acta Metallurgica Materialia 43(9):3459–3465

Warren WE (1987) Theoretical analysis of the double cleavage drilled compression specimen. Int J Fracture 33(3):223–235